Raytheon

VIIRS CLOUD MASK (VCM)

VISIBLE/INFRARED IMAGER/RADIOMETER SUITE ALGORITHM THEORETICAL BASIS DOCUMENT

Version 4: May 2001

Bonnie Reed

RAYTHEON SYSTEMS COMPANY
Information Technology and Scientific Services
4400 Forbes Boulevard
Lanham, MD 20706

SBRS Document #: Y2412

EDR: CLOUD MASK

Doc No: Y2412

Version: 4

Revision: 0

	Function	Name	Signature	Date
PREPARED BY	EDR DEVELOPER	B. REED		
APPROVED BY	RELEVANT LEAD	R. SLONAKER		
APPROVED BY	CHIEF SCIENTIST	S. MILLER		
RELEASED BY	ALGORITHM LEAD	P. KEALY		

TABLE OF CONTENTS

LIST OF FIGURES

Page

LIST OF TABLES

GLOSSARY OF ACRONYMS

ARM	Atmospheric Radiation Measurements
ADEOS2	Advanced Earth Observing Satellite-2
AERI	Atmospheric Emitted Radiance Inferometer
AERONET	Aerosol Robotic NETwork
AMSR	Advanced Microwave Scanning Radiometer
APOLLO	AVHRR Processing Scheme Over cloud Land and Ocean
ARMCAS	Arctic Radiation Measurement in Column: Atmosphere-Surface
ATBD	Algorithm Theoretical Basis Document
ATSR	Along-Track Scanning Radiometer
AVHRR	Advanced Very High Resolution Radiometer
AVIRIS	Airborne Visible Infrared Imaging Spectrometer
BBSS	Balloon-Borne Sounding System
BLC	Belfort Laser Ceilometer
BRDF	Bidirectional Reflectance Distribution Function
BRF	Bidirectional Reflectance Factor
BT	Brightness Temperature
BTD	Brightness Temperature Difference
CAR	Cloud Absorption Radiometer
CHAPS	Collocated HIRS/2 and AVHRR Processing Scheme
CLAVR	Clouds from AVHRR
CLS	Cloud Lidar System
CMIS	Conical Scanning Microwave Imager/Sounder
COARE	Coupled Ocean Atmosphere Response Experiment
CrIS	Cross-track Infrared Sounder
CSPOT	Cimel Sunphotometer
CVP	Cloud Validation Plan
DEM	Digital Elevation Model
DOC	Department of Commerce
DOD	Department of Defense
EDC	EROS Data Center
EDR	Environmental Data Record

EOS	Earth Observing System
EROS	Earth Resources Observation System
FIRE-ACE	First ISCPP Regional Experiment – Arctic Cloud Experiment
FOV	Field of View
FWHM	Full-width Half-maximum
GAC	Geological Association of Canada
GLI	Global Imager
GUV	Ground based Ultraviolet
HCS	Horizontal Cell Size
HITRAN	High Resolution Transmission Model
HSR	Horizontal Spatial Resolution
IABP	International Arctic Buoy Program
IPO	Integrated Project Office
IPT	Integrated Planning Team
IR	Infrared
IRT	Infrared Thermometer
LAC	Local Area Coverage
LANDSAT	Land Satellite
LLLS	Low Level Light Sensor
LUT	Look-Up Table
MAS	MODIS Airborne Simulator
MCM	MODIS Cloud Mask
MFRSR	Multi-Filter Rotating Shadowband Radiometer
MISR	Multiangle Imaging Spectroradiometer
MLP	Micropulse Lidar
MODIS	Moderate Resolution Imaging Spectroradiometer
MODTRAN	Moderate Resolution Atmospheric Radiance and Transmission Model
MWR	Microwave Water Radiometer
NASA	National Aeronautics and Space Administration
NDII	Normalized Differential Ice Index
NIP	Normal Incidence Pyrheliometer
NIR	Near Infrared

NOAA	National Oceanic and Atmosphere Administration
NPOESS	National Polar-orbiting Operational Environmental Satellite System
OMPS	Ozone Mapping Profiling Suite
PAN	Panchromatic
PSC	Polar Stratospheric Clouds
PSP	Precision Spectral Pyranometer
RDQI	Radiometric Data Quality Indicator
RGB	Red-Green-Blue
RL	CART Raman Lidar
RMS	Root Mean Square
RSS	Rotating Shadowband Spectrometer
SCARB	Smoke, Clouds, and Radiation – Brazil
SDR	Sensor Data Record
SERCAA	Support of Environmental Requirements for Cloud Analysis and Archive
SMET	Surface Meteorology
SMOS	Surface Meteorological Observation System
SNR	Signal-to-Noise Ratio
SRD	Sensor Requirements Document
SRR	Systems Requirements Review
SUCCESS	Subsonic Aircraft Contrail and Cloud Effects Special Study
TARFOX	Tropospheric Aerosol Radiative Forcing
TBD	To Be Determined
TBR	To Be Resolved
TOA	Top-of-Atmosphere
TOGA	Tropical Ocean Global Atmosphere
UAF	University of Alaska, Fairbanks
UV	Ultraviolet
UW	University of Wisconsin
VCM	VIIRS Cloud Mask
VIIRS	Visible/Infrared Imager/Radiometer Suite
VTLC	Video Time-Lapsed Camera
WINCE	Winter Cloud Experiment

ABSTRACT

The VIIRS Cloud Detection Algorithm determines if a given view of the Earth's surface is cloud-contaminated or cloud free. This detection results in the generation of a pixel-level cloudy/not cloudy mask at the HSR of the VIIRS sensor. This mask is an intermediate or ancillary data product for the retrieval of cloud and other EDRs (e.g., sea surface temperatures). To perform cloud detection the VIIRS radiance data for moderate resolution channels 0.67, 0.865, 1.37, 1.61, 3.7, 4.05, 8.55, 10.8, and 12.0 microns are used, the imagery resolution channels 0.645, 0.865, 1.61, 3.74, and 11.45 microns are used, as well as additional ancillary data.

The ancillary data required as input to the cloud detection algorithm include: sun/sensor geometry, global land/sea map, ecosystem map, geolocation data, sea surface winds, and the most recent snow/ice map.

Using the VIIRS radiance data in combination with the ancillary data the cloud detection is performed at both the imagery and moderate pixel resolution. The cloud detection involves a series of thresholding and ratioing tests using solar reflectance. The cloud detection also involves thresholding and differencing tests using the thermal Brightness Temperatures (BT). The threshold values for the various tests are dependent upon the dominant regional classification, or surface type, of the pixel to be tested. The tests applied to generate the cloud masks have a heritage from the Advanced Very High Resolution Radiometer (AVHRR) (Clouds from AVHRR [CLAVR], Stowe *et al*., 1995), and the Moderate Resolution Imaging Spectroradiometer (MODIS) (Ackerman *et al*., 1997).

1 INTRODUCTION

1.1 PURPOSE

This Algorithm Theoretical Basis Document (ATBD) describes the algorithm used to retrieve the Cloud Mask for the Visible/Infrared Imager/Radiometer Suite (VIIRS) instrument on the National Polar-orbiting Operational Environmental Satellite System (NPOESS). Specifically, this document identifies the sources of input data required for retrieval; provides the physical theory and mathematical background underlying the use of this information in the retrievals; includes implementation details; and describes assumptions and limitations of the proposed approach.

1.2 SCOPE

This document covers the algorithm theoretical basis for the cloud mask product of VIIRS on NPOESS. The VIIRS Cloud Mask (VCM) solution was developed using the MODIS and AVHRR cloud detection algorithm heritages.

Section 1 describes the purpose and scope of this document. Section 2 is an overview of the cloud mask. The theoretical description and implementation of the algorithm are described in Section 3, and the assumptions and limitations of the approach are summarized in Section 4. References for citations in the text are listed in Section 5.

1.3 VIIRS DOCUMENTS

This document contains references to other VIIRS documents. These are given in italicized brackets, e.g., *[V-29]* CLOUD MASK. The VIIRS documents cited in this document are listed below:

[V-0] VIIRS Experiment Overview

1.4 REVISIONS

This is the fourth version of this document dated May 2001; the first version was dated October 1998, the second version was dated June 1999, and the third version was dated May 2000.

2 EXPERIMENT OVERVIEW

2.1 OBJECTIVE OF VIIRS CLOUD MASK

The objective of the VCM is to determine whether clouds or optically thick aerosol obstructs a given view of the Earth surface, and whether a clear scene is contaminated by a shadow. The VCM is defined as the pixel level flag that indicates when a cloud intersects a line segment extending between the sensor and a given area of the Earth's surface. The VCM operates at a moderate pixel resolution (750 m), and at the imagery pixel resolution (375 m). Input to the cloud mask algorithm is assumed to be calibrated and navigated VIIRS radiance data and ancillary data. Additionally, the VIIRS data are assumed to meet instrument specifications so that no accommodation for striping or poor navigation is required.

Our approach to the VCM is for each pixel to provide a confidence flag that indicates how certain we are that the pixel is clear. The cloud masking algorithm must operate under the following restrictions: near-real time execution, limited computer storage, and simplicity so that many users can follow the algorithm path.

2.2 INSTRUMENT CHARACTERISTICS

The VIIRS bands used in the cloud mask algorithm are identified in Table 1.

Table 1 VIIRS bands used in the VCM algorithm

Band	Wavelength (μm)	Used in Cloud Mask
DNB	0.700	N
M1	0.4120	N
M2	0.4450	N
M3	0.4880	N
M4	0.5550	N
I1	0.6450	Y
M5	0.6720	Y
M6	0.7510	N
I2	0.8650	Y
M7	0.8650	Y
M8	1.2400	N
M9	1.3780	Y
I3	1.610	Y
M10	1.160	Y
M11	2.2500	N

Band	Wavelength (μm)	Used in Cloud Mask
M12	3.700	Y
I4	3.7400	Y
M13	4.0500	Y
M14	8.5500	Y
M15	10.7625	Y
I5	11.4500	Y
M16	12.0125	Y

Additional details on the instrument design are provided in the VIIRS Experiment Overview *[V-0]*.

2.3 HISTORICAL PERSPECTIVE

The VCM is essentially derived from the MODIS Cloud Mask (MCM) mulit-channel cloud masking techniques, which in turn have their heritage in previously developed algorithms. The International Satellite Cloud Climatology Project (ISCCP) has developed cloud detection schemes using visible and infrared window radiances. The AVHRR (Advanced Very High Resolution Radiometer) Processing scheme Over cLoud Land and Ocean (APOLLO) cloud detection algorithm uses the five visible and infrared channels of the AVHRR. The NOAA Cloud Advanced Very High Resolution Radiometer (CLAVR) also uses a series of spectral and spatial variability tests to detect a cloud. Additionally, spatial coherence of infrared radiances in cloudy and clear skies has been used successfully in regional cloud studies.

The above algorithms are noted as they have been incorporated into current global cloud climatologies and have been run in an operational mode over long time periods. The VCM algorithm builds on this work, but has considerable advantage because it has multispectral information and conducts tests at the imagery and moderate resolutions. VIIRS has 375 m imagery resolution in five channels and 750 m moderate resolution in 16 channels and both resolutions include channels in the visible, near-infrared, and infrared.

3 ALGORITHM DESCRIPTION

3.1 PROCESSING OUTLINE

The current processing outline (See Figure 1) is based on the MODIS current operational approaches. The VCM uses VIIRS data and ancillary data as input to produce a variety of output flags. The VCM output is used by many EDRs that are dependent on cloud masking. The VCM performs cloud tests at both the radiometric resolution, using the radiometric bands, and at the higher imagery resolution.

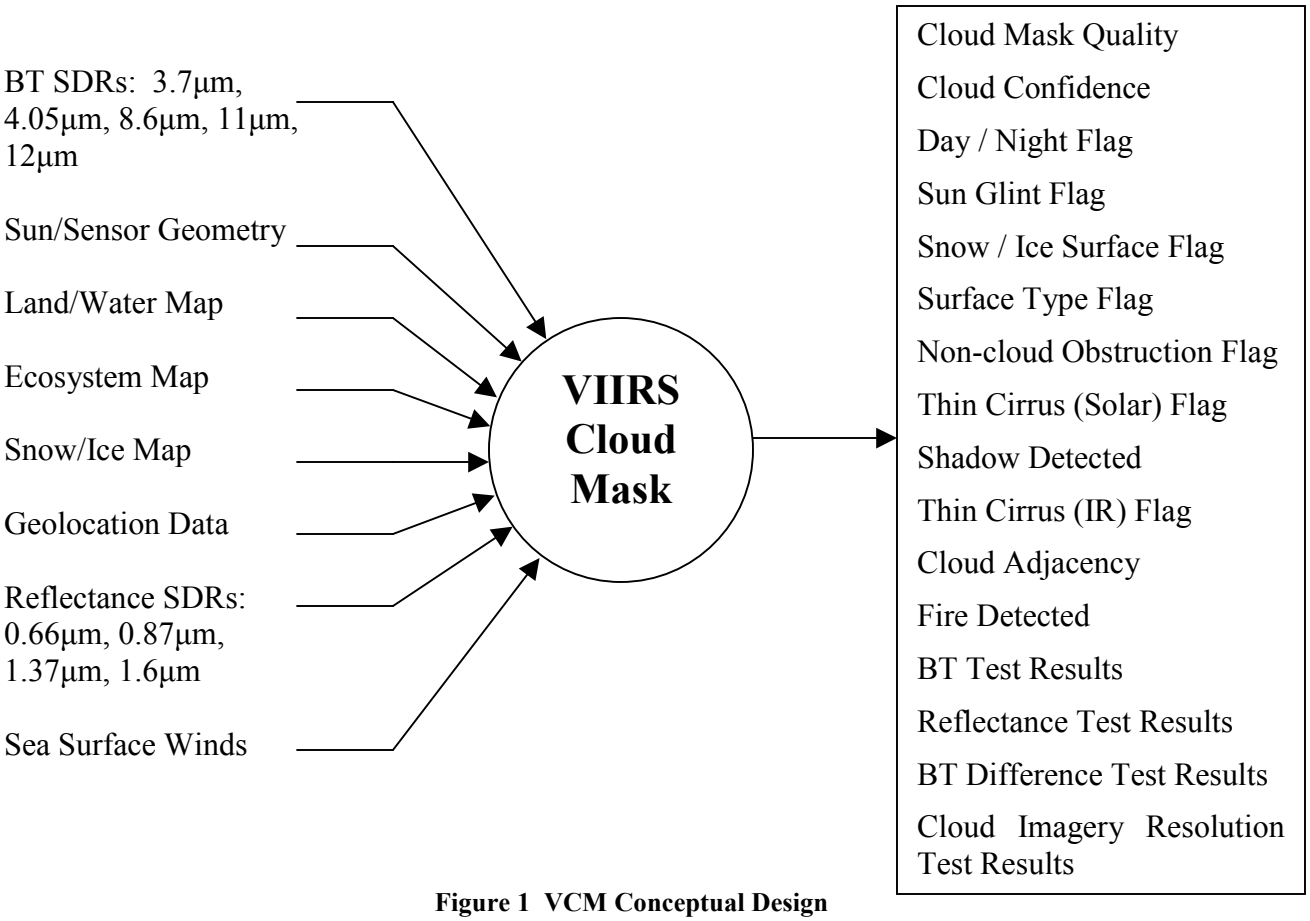

Figure 1 VCM Conceptual Design

3.2 ALGORITHM INPUT

The algorithm requires ancillary information from the VIIRS instrument and from outside sources. All of the input data are explained in greater detail in the following section.

Table 2 Ancillary data inputs for the VCM

Input Data	Source of Data
VIIRS calibrated TOA Brightness Temperatures SDR	VIIRS
VIIRS calibrated TOA Reflectance SDR	VIIRS
Sun / Sensor Geometry: Solar Zenith Angle, Azimuthal Angle, and Viewing Angle	VIIRS
Snow / Ice Map	VIIRS
Geolocation Data	VIIRS
Land / Water Map at 1 km Resolution	EROS Data Center
Ecosystem Map	Olson/Loveland
Sea Surface Winds	CMIS/NCEP

3.2.1 VIIRS Data

As indicated earlier, input to the cloud mask algorithm is assumed to be calibrated and navigated VIIRS radiance data. Additionally, the cloud mask requires several ancillary data inputs.

3.2.1.1 VIIRS calibrated TOA Brightness Temperatures SDR

The cloud mask performs several infrared window threshold brightness temperature techniques for cloud detection and the VIIRS calibrated TOA brightness temperatures SDR is needed to execute these tests.

3.2.1.2 VIIRS calibrated TOA Reflectance SDR

The cloud mask uses reflectance data techniques for cloud detection and the VIIRS calibrated TOA reflectance SDR is needed to carry out these techniques.

3.2.1.3 Sun / Sensor Geometry

The sun viewing geometry and the sensor viewing geometry are required for the VCM. These are used for setting some reflectance threshold tests. The data will be used to look for sun glint effects; set, apply, or adjust thresholds for cloud detection tests; assist in eliminating optically thick aerosol-laden paths (which can be misidentified as clouds); assist in the identification of cloud shadows; and to determine if a pixel is in the day or night regime. The night regime is defined as when the solar zenith angle exceeds 85 degrees.

3.2.1.4 Snow / Ice Map

The snow/ice map is needed to decide which cloud detection tests will be applied, and to adjust thresholds of several tests. Spectrally, snow/ice and clouds have many similar features. A snow/ice map will be obtained from the previous 12 hour VIIRS Snow Cover EDR result. The snow/ice map will decrease the misclassification of snow/ice as clouds.

3.2.1.5 Geolocation Data

The surface coordinates (latitude and longitude) allow the land/sea/ecosystem information to be obtained from the land/water and ecosystems maps.

3.2.2 Non-VIIRS Data

The non-VIIRS data that the VCM uses is provided by several different sources and is described in the following subsections.

3.2.2.1 Land / Water Map

The VCM requires a land/water map to discriminate land from water. Land and water possess different surface reflective properties. These properties affect the thresholds applied in discriminating clear sky from cloud. The land/water map will be provided by the EROS Data Center.

3.2.2.2 Ecosystem Map

Various land types possess different reflective properties. The reflective properties need to be known to properly develop and identify the correct thresholds to be applied in cloud tests. The Olson map of ecosystems (10 minute resolution) is being used for global processing, while Tom Loveland's ecosystem map (1 km resolution) is being applied while over North America.

3.2.2.3 Sea Surface Winds

Sea surface winds need to be analyzed when detecting sun glint. Therefore, sea surface wind data is needed to determine if detected sun glint is a function of surface wind. Sea surface wind data will be obtained from the current CMIS data collection results. If CMIS data are unavailable, sea surface wind data will be obtained from NCEP sea surface analysis.

3.3 ALGORITHM OUTPUT

The output of the VCM algorithm will be 6 bytes (48 bits) for each moderate resolution pixel. The mask includes information about the processing path the masking took (e.g., land or ocean) and whether a view of the surface is obstructed. A potentially large number of applications will use the cloud mask and some algorithms will be more tolerant of cloud contamination than others. For example, some algorithms may apply a correction to account for the radiative effects

of a thin cloud. In addition, certain algorithms may use spectral channels that are more sensitive to the presence of clouds than others.

The boundary between defining a pixel as cloudy or clear is sometimes ambiguous. For example, a pixel may be partly cloudy, or a pixel may appear as cloudy in one spectral channel and appear cloud-free at a different wavelength. Figure 2 shows three spectral images of a subvisual contrail taken from the MAS during the Subsonic Aircraft Contrail and Cloud Effects Special Study (SUCCESS). The left most panel is a MAS image in the 0.66 μm channel, a spectral channel typical of many satellites and commonly used for land surface classifications such as the NDVI. The contrail is not discernible in this image and scattering effects of the radiation may be accounted for in an appropriate atmospheric correction algorithm. The right most panel is a MAS 11 μm image (dark is cold, light is warm). Evidence of a contrail lingers though it would be difficult to justify its existence without the aid of the center panel, which is an image obtained using the 1.88 μm channel. The 1.88 μm spectral channel is near a strong water vapor absorption band and, during the day, is extremely sensitive to the presence of high level clouds. The 1.88 μm channel is comparable to the VIIRS 1.38 μm channel. While the contrail seems to have little impact on visible reflectance, its effect in the infrared window is enough to affect the retrievals of surface temperature. In this type of scene, the cloud mask needs to provide enough information to be useful to both visible and infrared applications.

Figure 2 Three spectral images (0.66, 1.88 and 11 um) taken from the MAS during the SUCCESS experiment (20 April 1996).

To allow for the imprecise measurement of the real world and to accommodate a wide variety of applications, the mask is more than a simple yes/no decision (though bit 1 alone could be used to represent a single bit cloud mask). The cloud mask includes 4 levels of 'confidence' (bits 1 and 2)[1] with regard to whether a pixel is thought to be clear as well as the results from different spectral tests. The bit structure of the cloud mask is described in Table 3 and a description of the bit fields follow.

[1] In this document, representations of bit fields are ordered from right to left. Bit 0, or the right-most bit, is the least significant.

Table 3 File specification for the 48-bit VCM

BIT FIELD	FLAG DESCRIPTION KEY	RESULT
0	Cloud Mask Quality	0 = Questionable 1 = Okay
1-2	Cloud Confidence	00 = Confident Cloudy 01 = Probably Cloudy 10 = Probably Clear 11 = Confident Clear
3	Day / Night	0 = Night 1 = Day
4-5	Sun Glint	00 = Geometry Based Sunglint 10 = Wind Speed Based Sunglint 11 = No Sunglint (One spare flag, 01)
6	Snow / Ice Surface	0 = Snow/Ice 1 = No Snow/Ice
7-8	Land / Water Background	00 = Water 01 = Land and Water (Coastal) 10 = Land and Desert 11 = Land no Desert
9	Non Cloud Obstruction (Heavy Aerosol) (BT_{11}-BT_{12})	0 = Yes 1 = No
10	Thin Cirrus Detection (Solar) ($R_{1.38}$)	0 = Yes 1 = No
11	Shadow Detected	0 = Yes 1 = No
12	Thin Cirrus Detection (IR) (BT_{11}-BT_{12}; $BT_{3.7}$-BT_{12})	0 = Yes 1 = No
13	Cloud Adjacency	0 = Yes 1 = No
14	Fire Detected ($BT_{4.05}$ & $BT_{4.05}$-BT_{11})	0 = Yes 1 = No

BIT FIELD	FLAG DESCRIPTION KEY	RESULT
15	IR Threshold Cloud Test (BT_{11})	0 = Yes 1 = No
16	High Cloud Flag ($R_{1.38}$) Test	0 = Yes 1 = No
17	High Cloud ($BT_{3.7}$ - BT_{12}) Test	0 = Yes 1 = No
18	IR Temperature Difference Test ($BT_{8.6}$- BT_{11}& BT_{11}- BT_{12})	0 = Yes 1 = No
19	Temperature Difference Test (BT_{11}- $BT_{3.7}$)	0 = Yes 1 = No
20	Visible Reflectance Test ($R_{0.66}$ or $R_{0.87}$)	0 = Yes 1 = No
21	Visible Ratio Test ($R_{0.87}$/ $R_{0.66}$)	0 = Yes 1 = No
22	Temperature Difference Test ($BT_{3.7}$ –$BT_{4.05}$)	0 = Yes 1 = No
23-26	Cloud Imagery Resolution Test 1	0000 = Cloudy 1111 = Not Cloudy Each bit is a pixel of the 2x2 imagery resolution pixels nested in the radiometric resolution pixel: 0000 = all cloudy, 1111 = all clear
27-30	Cloud Imagery Resolution Test 2	See Test 1 Result
31-34	Cloud Imagery Resolution Test 3	See Test 1 Result
35-38	Cloud Imagery Resolution Test 4	See Test 1 Result
39-47	Spare	Spare Bits

3.3.1 Bit 0 – Cloud Mask Quality

Since VIIRS produces a cloud mask in any situation, a quality flag is attached to the final cloud mask. This bit will indicate whether the cloud mask is questionable (0) or okay (1). A questionable cloud mask may stem from bad radiance data, which would cause erroneous test results.

3.3.2 Bits 1-2 -- Cloud Confidence

Confidence flags convey strength of conviction in the outcome of the cloud mask algorithm tests for a given FOV. When performing spectral tests, as one approaches a threshold limit, the certainty or confidence in the outcome is reduced. Therefore, a confidence flag for each individual test, based upon proximity to the threshold value, is assigned and used to work towards a final quality flag determination for the FOV. The current scheme applies a linear interpolation between a low confidence clear threshold and high confidence clear threshold for each spectral test.

The final determination is a combination of the confidences of all applied tests. This determination will dictate whether additional testing is warranted to improve the confidence. The final cloud mask determination will be clear or cloudy with a confidence level associated with it. If any consistency test fails, the confidence in the final cloud/no cloud determination is reduced.

3.3.3 Bit 3 – Day / Night Flag

A combination of solar zenith angle and instrument mode (day or night mode) at the pixel latitude and longitude at the time of the observations are used to determine if a daytime or nighttime cloud masking algorithm should be applied. Daytime algorithms, which include solar reflectance data, are constrained to solar zenith angles less than 85°. If this bit is set to 1, daytime algorithms were executed.

3.3.4 Bits 4-5 – Sun Glint Flag

Sun glint processing path is taken when the reflected sun angle, θ_r, lies between 0° and approximately 36°, where

$$\cos\theta_r = \sin\theta \sin\theta_0 \cos\phi + \cos\theta \cos\theta_0,$$

where θ_0 is the solar zenith angle, θ is the viewing zenith angle, and ϕ is the azimuthal angle. Sun glint is also a function of surface wind and sea state.

3.3.5 Bit 6 – Snow / Ice Surface Flag

Certain cloud detection tests (e.g., visible reflectance tests) are applied differently in the presence of snow or ice. This bit is set to a value of 0 when the cloud mask processing algorithm assumes that snow is present. This bit indicates a processing path and if set to 1 it should not be interpreted that snow/ice is on the ground.

3.3.6 Bits 7-8 – Surface Type Flag

The three surface type flag bits of the cloud mask output file contain information concerning the processing path taken through the algorithm. There are four possible surface type processing paths: water, land and water (coastal), land and desert, or land no desert.

Thresholds for the spectral tests are a function of surface background, land and water being the two most obvious. Therefore, each pixel will be tagged as being land or water. Presently the VCM uses the 1 km resolution world map provided from the EROS Data Center (EDC).

Some cloud detection algorithms are also ecosystem dependent. Thus, an ecosystem will be determined for each land pixel. Over North America the current version of the cloud mask uses Tom Loveland's 1 km ecosystem map. Global applications currently use the 10-minute resolution Olson World Ecosystem map.

3.3.7 Bit 9 – Non-cloud Obstruction

Smoke from forest fires, dust storms over deserts, and other aerosols that result in obstructing the FOV between the surface and the satellite may be flagged as "cloud." The aerosol obstruction bit will be set to zero if simple spectral tests indicate the possible presence of aerosols.

3.3.8 Bit 10 – Thin Cirrus Detected (Solar)

VIIRS includes a unique spectral channel, 1.38 μm, specifically included for the detection of thin cirrus. Land and sea surface retrieval algorithms may attempt to correct the observed radiances for the effects of thin cirrus. If this bit is set to 0, thin cirrus was detected using this channel.

3.3.9 Bit 11 – Shadow Detected

Some land retrieval products are as sensitive to the presence of shadows as they are to contamination by thin clouds. The VIIRS Cloud Masking algorithm checks for the presence of a shadow whenever bits 1 and 2 are greater than 00. If bit 12 is set to zero, a shadow was detected using spectral tests. If bits 1 and 2 are 00 (confident cloudy), tests will be run to discern if a shadow from a high cloud is being cast on a lower cloud. If such a case is detected, this bit is set to 1.

3.3.10 Bit 12 – Thin Cirrus Detected (IR)

Through brightness temperature differencing techniques, the VIIRS Cloud Masking algorithm checks for the presence of thin clouds in the upper troposphere. These cloud tests are independent of the "Thin Cirrus Detection" bit. If thin cirrus was detected using IR channels, the flag is set to 0.

3.3.11 Bit 13 – Cloud Adjacency

If a pixel is clear, adjacent pixels will be searched to determine if any are low confidence clear. If so, this bit will be set to 0.

3.3.12 Bit 14 – Fire Detected

The fire detection bit is modeled after the MODIS fire detection algorithm. The fire detection strategy is based on absolute detection of the fire (if the fire is strong enough) and on detection relative to the background to account for variability of the surface temperature and reflection by sunlight.

3.3.13 Bits 15-22 – Cloud Tests Results

These bits represent the results of individual cloud detection tests. Each individual test is discussed in the next section.

3.3.14 Bits 23-38– Cloud Imagery Resolution

The VIIRS Imagery resolution bands 'nest' in the moderate resolution bands as is depicted in Figure 3.

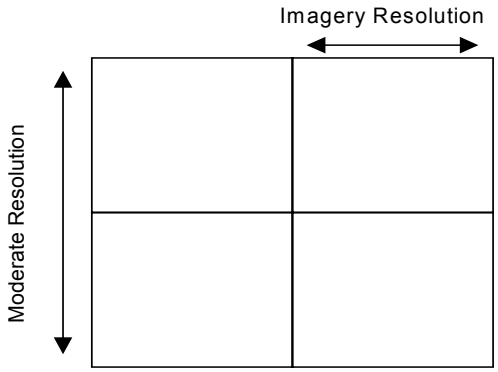

Figure 3 Depiction of the Nesting of the VIIRS Imagery Resolution Bands within the VIIRS Moderate Resolution Bands

This nesting allows the inclusion of an imagery resolution cloud mask along with the VCM output. The individual imagery resolution pixels, 4 of which are contained within a given moderate resolution pixel, undergo cloud detection tests, and the 2x2 imagery pixel regions have spatial contrast tests done to them which are of CLAVR heritage. For the 48 bit output IP the 4 bits are ordered from the upper left imagery resolution quadrant. The first bit is this upper left quadrant, the second bit is the upper right quadrant, the third bit is the lower left quadrant, and the fourth bit is the lower right quadrant.

3.3.15 Bits 39 -47 – Spare Bits

These spare bits are reserved for future tests not yet devised.

3.4 CONFIDENCE FLAGS

Most of the single pixel tests rely on thresholds. Thresholds are never global. There are always exceptions. For example, the ratio of reflectance at 0.87 to 0.66 μm identifies cloud for values in the range $0.9 < R_{0.87}/R_{0.66} < 1.1$. It seems unrealistic to label a pixel with $R_{0.87}/R_{0.66} = 1.09$ as cloudy, and a neighboring pixel with the ratio of 1.11 as non-cloudy. Rather, as one approaches the threshold limits, the certainty or confidence in the labeling becomes more and more uncertain. An individual confidence flag is assigned to each single pixel test and is a function of how close the observation is to the thresholds. The individual confidence flags are combined to produce the final cloud mask flag for the output file.

The uncertainty is a function of instrument noise in that channel and the magnitude of the correction that was necessary due to surface spectral radiative properties, as well as atmospheric moisture and/or aerosol reflection contributions. The individual confidence flag will indicate a confidence level for each single pixel test result. The initial FOV obstruction determination is an amalgamation of all confidence flags and single pixel test results. This determination will dictate whether additional testing is warranted to improve the confidence. The final cloud mask determination is a clear-sky confidence with one of four levels associated with it: confidently clear, probably clear, probably cloudy and confidently cloudy. This approach quantifies our confidence in the derived cloud mask for a given pixel. This section describes the method of assigning a confidence to a given spectral test.

Many cloud detection schemes have a single threshold for a given test. For example, if the visible reflectance over the ocean is greater than 6% then the pixel is set to cloudy. The cloud masking is designed to provide information on how much confidence a user can place on the result. Each test is assigned a value between 0 and 1 representing increasing confidence in clear-sky conditions. Figure 4 is a graphical representation of how a confidence level is assigned for a spectral test. The abscissa represents the observation and the ordinate the clear-sky confidence level. In this test, an observation greater than a value of γ is determined to be a high confidence clear scene and assigned a value of 1. An observation with a value less than α is cloudy and assigned a confidence level of 0. These high confidence clear and cloud thresholds, γ and α respectively, are determined from observations and/or theoretical simulations.

Values between α and γ are assigned a value between 0 and 1 (or 1 and 0). Assignment is based on a linear function. Experiments have been performed with assigning confidence values based on S-functions:

$$S(x;\alpha,\beta,\gamma)=\begin{cases}0 & \text{for } x\le\alpha\\ 2\left(\dfrac{x-\alpha}{\gamma-\alpha}\right)^2 & \text{for } \alpha\le x\le\beta\\ 1-2\left(\dfrac{x-\alpha}{\gamma-\alpha}\right)^2 & \text{for } \beta\le x\le\gamma\\ 1 & \text{for } x\ge\gamma\end{cases}$$

The S-function is quadratic between the points α and γ. If the '2' exponent in the above equation is replaced with a 1, then the S-function becomes linear. Experiments indicate that changing between a quadratic and linear function primarily affects cloud masking at the edge of cloud systems. For simplicity we have stayed with the linear function.

In the final cloud mask only four levels of confidence are provided; confident clear, probably clear, probably cloudy, and confident cloudy.

The β value in Figure 4 is the pass/fail threshold for a given test. Each test therefore has a minimum of three thresholds value for pass/fail, high confidence pass and high confidence fail. Some tests, such as the visible ratio test, identify cloud if the observations fall within a given range (e.g., $0.9 < R_{0.87}/ R_{0.66} < 1.1$). For these range tests there are six thresholds, three for each end.

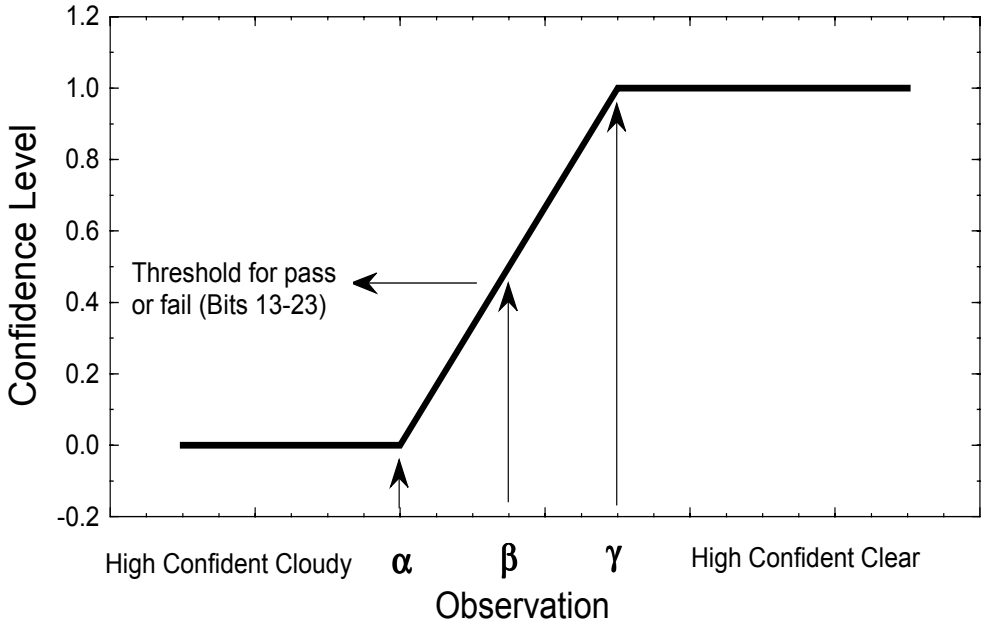

Figure 4 A graphical depiction of three thresholds used in cloud screening

3.5 THEORETICAL DESCRIPTION OF CLOUD DETECTION

This section discusses the physics of detecting clouds using multispectral radiances from a given field of view (FOV) or an array of FOVs, presents the application with VIIRS data, and indicates various problem areas.

3.5.1 Physics of the Problem

Clouds are generally characterized by higher reflectance and lower temperature than the underlying earth surface. As such, simple visible and infrared window threshold approaches offer considerable skill in cloud detection. However, there are many surface conditions when this characterization of clouds is inappropriate, most notably over snow and ice. Additionally, some cloud types such as thin cirrus, low stratus at night, and small cumulus are difficult to detect because of insufficient contrast with the surface radiance. Cloud edges cause further difficulty since the instrument field of view will not always be completely cloudy or clear.

3.5.2 Infrared Brightness Temperature Thresholds and Difference (BTD) Tests

Several infrared window threshold and temperature difference techniques have been developed. These algorithms are most effective at night for cold clouds over water and must be used with caution in other situations.

3.5.2.1 IR Threshold Cloud Test - BT_{11} (Bit 15)

The first infrared test to apply over the oceans is a simple threshold test. Over open ocean when the brightness temperature in the 11 μm (BT_{11}) channel (band M15) is less than 270 K, we assume the pixel to fail the clear-sky condition. With reference to Figure 4, the three thresholds over ocean are 267, 270, and 273 K, respectively, as shown in Figure 5.

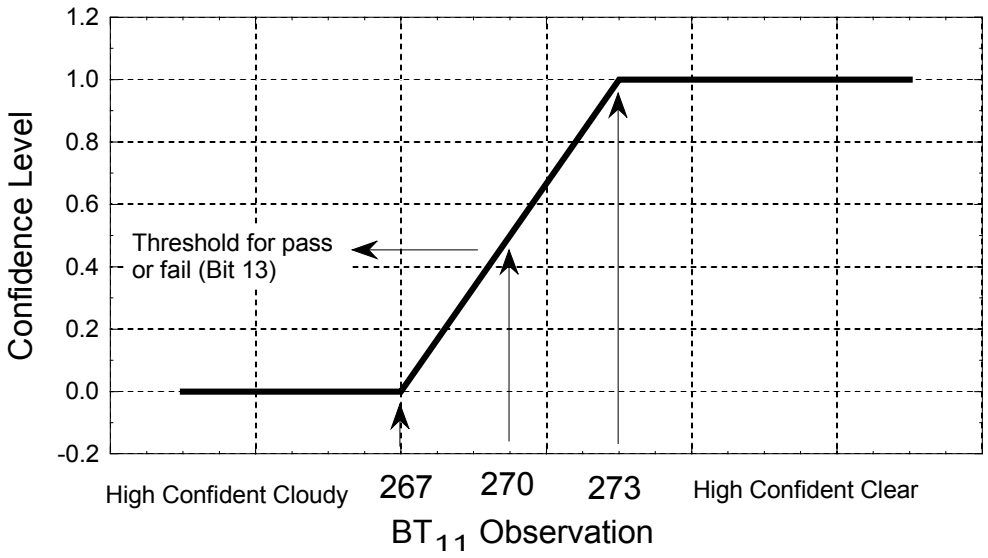

Figure 5 Thresholds for the simple IR window cold cloud test

Cloud masking over land surface from thermal infrared bands is more difficult than over ocean due to potentially larger variations in surface emittance. Nonetheless, simple thresholds can be established over certain land features. For example, over desert regions we can expect that BT_{11}< 273K denotes cloud. Such simple thresholds will vary with ecosystem, season, and time of day.

3.5.2.2 High Cloud Test - $BT_{3.7} - BT_{12}$ (Bit 17)

This window brightness temperature difference test is applied during the nighttime over some, but not all, surfaces. This difference is useful for separating thin cirrus and cloud free condition and is relatively insensitive to the amount of water vapor in the atmosphere (Hutchison and Hardy 1995).

3.5.2.3 Tri-Spectral Cloud Test - $BT_{8.6} - BT_{11}$ and $BT_{11} - BT_{12}$ (Bit 18)

As a result of the relative spectral uniformity of surface emittance in the IR, spectral tests within various atmospheric windows (such as bands M14, M15, and M16 at 8.6, 11, and 12 μm, respectively) can be used to detect the presence of cloud. Differences between $BT_{11}$and BT_{12} are widely used for cloud screening with AVHRR measurements, and this technique is often referred to as the split window technique. Saunders and Kriebel (1988) used BT_{11}- BT_{12} differences to detect cirrus clouds. Brightness temperature differences are greater over thin clouds than over clear or overcast conditions. Cloud thresholds were set as a function of satellite zenith angle and

the BT_{11}brightness temperature. Inoue (1987) also used BT_{11}- BT_{12} versus BT_{11} to separate clear from cloudy conditions.

In difference techniques, the measured radiances at two wavelengths are converted to brightness temperatures and subtracted. Because of the wavelength dependence of optical thickness and the non-linear nature of the Planck function (B_λ), the two brightness temperatures are often different. Figure 6 is an example of a theoretical simulation of the brightness temperature difference between 11 and 12 μm versus the brightness temperature at 11 μm, assuming a standard tropical atmosphere. The difference is a function of cloud optical thickness and the cloud particle size distribution. The difficulty is often defining the clear-sky value on this type of diagram.

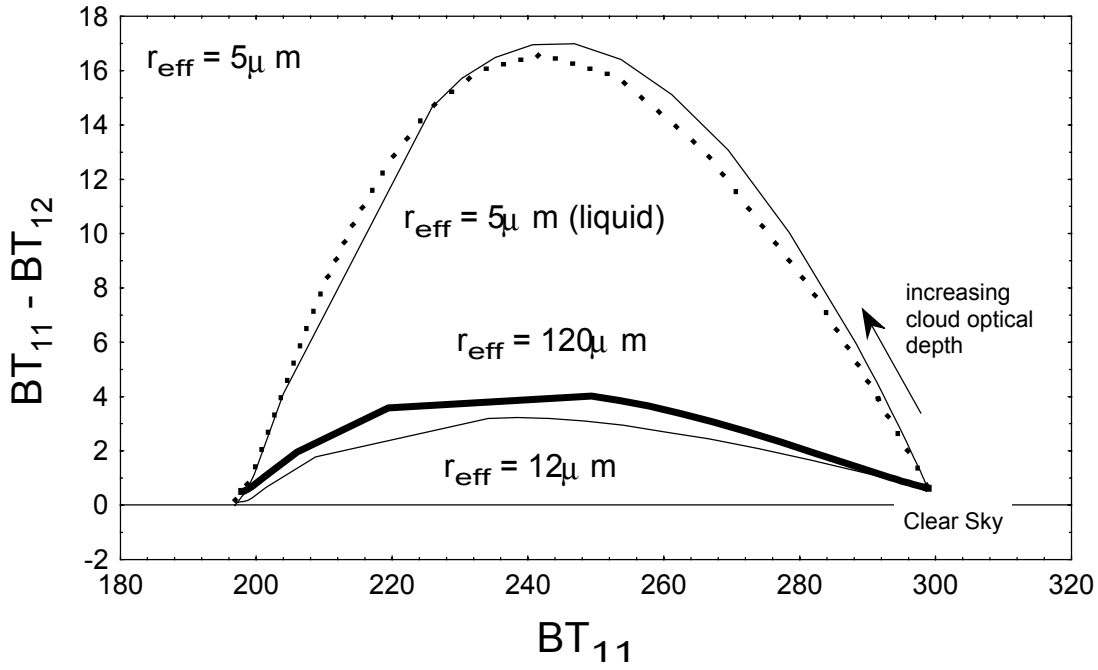

Figure 6 Theoretical simulations of the brightness temperature difference as a function of $BT_{11}$for a cirrus cloud of varying cloud microphysical properties

The basis of the split window and tri-spectral technique for cloud detection lies in the differential water vapor absorption that exists between different window channel (8.6 and 11 μm and 11 and 12 μm) bands. These spectral regions are considered to be part of the atmospheric window, where absorption is relatively weak. Most of the absorption lines are a result of water vapor molecules, with a minimum occurring around 11 μm. Since the absorption is weak, BT_{11} can be corrected for moisture absorption by adding the scaled brightness temperature difference of two spectrally close channels with different water vapor absorption coefficients; the scaling coefficient is a function of the differential water vapor absorption between the two channels.

VIIRS has a unique capability since it has measurements at three wavelengths in the window, 8.6, 11, and 12 μm. The three spectral regions mentioned are very useful in determination of cloud free atmospheres. Because the index of refraction varies quite markedly over this spectral region for water, ice, and minerals common to many naturally occurring aerosols, the effect on the brightness temperature of each of the spectral regions is different, depending on the absorbing constituent.

Ackerman et al. (1990) suggested a tri-spectral combination of observations at 8.6, 11 and 12 μm for detecting cloud properties. Strabala et al. (1994) further explored this technique by utilizing very high spatial-resolution data from MAS. The physical premise of the technique is that ice and water vapor absorption peak in opposite halves of the window region; so that positive 8.6 minus 11 μm brightness temperature differences indicate cloud while negative differences, over oceans, indicate clear regions. The relationship between the two brightness temperature differences and clear-sky have also been examined using collocated HIRS and AVHRR GAC global ocean data sets. As the atmospheric moisture increases, $BT_{8.6} - BT_{11}$ decreases while $BT_{11} - BT_{12}$ increases.

Figure 7 demonstrates a relationship between BT_{11} - BT_{12} and BT_8- BT_{11} using collocated AVHRR and HIRS/2 observations.

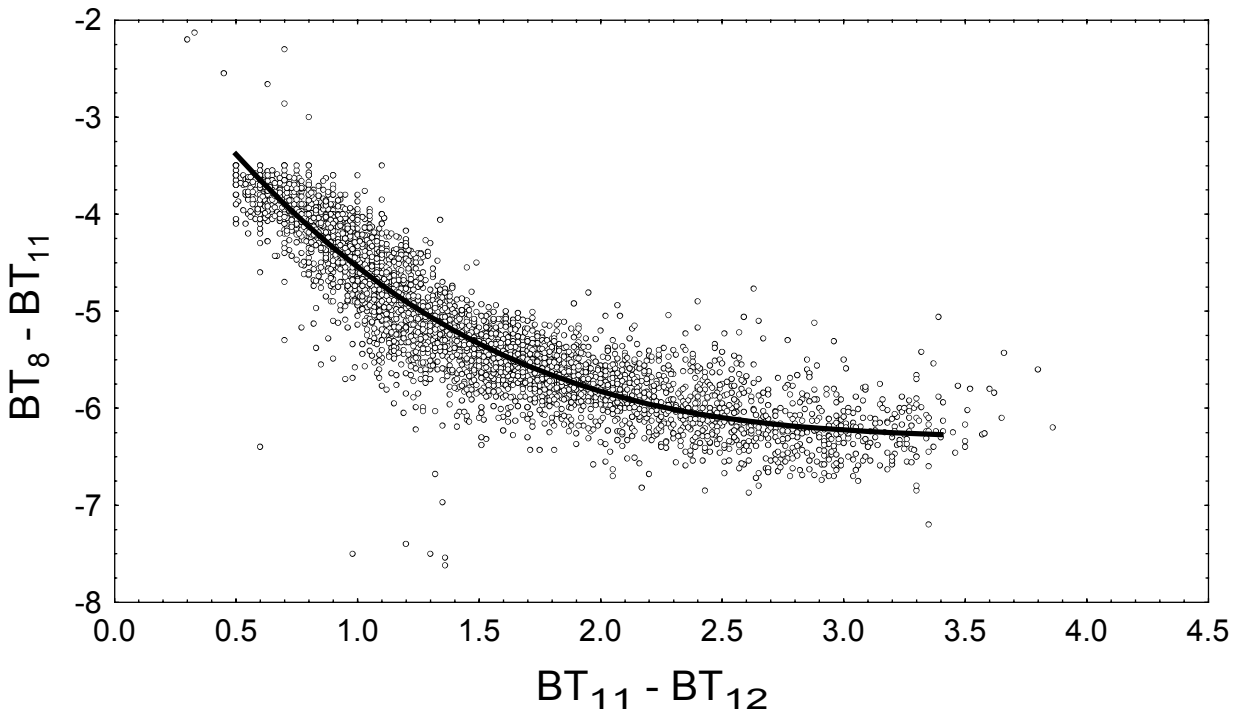

Figure 7 The tri-spectral diagram for clear-sky ocean scenes

Brightness temperature difference testing can also be applied over land with careful consideration of variation in spectral emittance. For example, $BT_{11} - BT_{8.6}$ has large negative

values over daytime desert and is driven to positive differences in the presence of cirrus. Some land regions have an advantage over ocean regions because of the larger number of surface observations, including air temperature and vertical profiles of moisture and temperature.

3.5.2.4 Cloud Test - $BT_{11} - BT_{3.7}$ (Bit 19)

The difference between BT_{11} and $BT_{3.7}$ can be used to detect the presence of clouds. At night the difference between the brightness temperatures measured in the shortwave (3.7 μm) and in the longwave (11 μm) window regions ($BT_{11} - BT_{3.7}$) can be used to detect partial cloud or thin cloud within the VIIRS field of view. Small or negative differences are observed only for the case where an opaque scene (such as thick cloud or the surface) fills the field of view of the sensor. Negative differences occur at night over extended clouds due to the lower cloud emissivity at 3.7 μm.

During the daylight hours the difference between BT_{11} and $BT_{3.7}$ is a large negative because of reflection of solar energy at 3.7 μm. This technique is very successful at detecting low level water clouds. $BT_{11} - BT_{3.7}$ is not applied over deserts during daytime or nighttime, as bright desert regions with highly variable emissivities tend to be classified incorrectly as cloudy with this test. Experience indicates that the actual thresholds will need to be adjusted for ecosystem type.

Moderate to large differences between BT_{11} and $BT_{3.7}$ result when a non-uniform scene (e.g., broken cloud) is observed. The different spectral responses to a scene of non-uniform temperature are a result of Planck's law. The brightness temperature test is dependent on the warmer portion of the scene increasing with decreasing wavelength. Differences in the brightness temperatures of the longwave and shortwave channels are small when viewing mostly clear or mostly cloudy scenes; however, for intermediate situations the differences become large (greater than 3°C). Table 4 lists the thresholds used, which are of MODIS heritage.

Infrared window tests at high latitudes are difficult. Distinguishing clear and cloud regions from satellite IR radiances is a challenging problem due to the cold surface temperatures. Yamanouchi et al. (1987) describe a nighttime polar (Antarctic) cloud/surface discrimination algorithm based upon brightness temperature differences between the AVHRR 3.7 and 11 μm channels and between the 11 and 12 μm channels. Their cloud/surface discrimination algorithm was more effective over water surfaces than over inland snow-covered surfaces. A number of problems arose over inland snow-covered surfaces. First, the temperature contrast between the cloud and snow surface became especially small, leading to a small brightness temperature difference between the two infrared channels. Second, the AVHRR channels are not well-calibrated at extremely cold temperatures (< 200 K).

Table 4 Thresholds used for BT_{11} - $BT_{3.7}$ test for low cloud in the VIIRS cloud mask algorithm

Scene Type	Threshold	High confidence clear	Low confidence clear
Day ocean	-8.0 K	-6.0 K	-10.0 K
Night ocean	0.60 K	0.50 K	0.70 K
Day land	-12.0 K	-10.0 K	-14.0 K
Night land	0.60 K	0.50 K	0.70 K
Day snow/ice	-9.0 K	-7.0 K	-11.0 K
Night snow/ice	0.60 K	0.50 K	0.70 K

3.5.2.5 Cloud Detection Test - $BT_{3.7} - BT_{4.05}$ (Bit 22)

Performing this *BT* difference test is another method of removing the solar and thermal contribution of the 3.7 μm channel. Due to the small wavelength differences between these two bands the thermal contribution due to temperatures within a pixel are relatively close. The largest difference between these two bands is the solar component in the 3.7 μm channel. The difference removes the BT resulting from the solar component of 3.7 μm alone. Due to both the low reflectance of most surface types, and the relative high reflectance of clouds in the 3.7 μm channel this test has demonstrated much promise in MAS data.

3.5.3 Sun Glint Test (Bits 4-5)

Sun glint pixels possess glitter contamination. Consequently, the pixels in which possible sun glint is occurring need to be identified. Solar channel threshold values need to be adjusted for these pixels. Sun glint will not result in a cloud mask being generated. In the case of sun glint the solar tests performance may be inhibited, but the thermal channel tests will still be done to generate the equivalent of a nighttime cloud mask. Knowledge of sea surface winds are included in the sun glint test, surface winds can narrow the region in which sun glint may occur. There is a justifiable concern that cloud detection will not be as reliable in glitter-contaminated regions. A classification as clear is probably correct, but a classification as cloudy may actually be due to the glitter effect as opposed to a cloud. Sun glint will be considered over both land and water areas. Land regions are included because spatially unresolved water bodies, snow, or recent rainfall can also cause sun glint.

Sun glint may occur when the reflected sun angle θ_r, is 0° to 36°, where:

$$\cos\theta_r = \sin\theta \sin\theta_o \cos\phi + \cos\theta \cos\theta_o$$

Where θ_o is the solar zenith angle, θ is the viewing zenith angle, and ϕ is the azimuthal angle.

Sun glint is also a function of the state of the ocean, and effected by sea surface winds.

3.5.4 Non-cloud Obstruction Test (Bit 9)

A heavy aerosol laden atmosphere may result in a low confidence clear scene. Certain simple tests may be constructed that can indicate that the FOV is contaminated with an aerosol and not a cloud. For example, negative values of $BT_{11} - BT_{12}$ are often observed over deserts and can be attributed to the presence of dust storms (Ackerman 1996). Under such conditions, provided BT_{11} is warm, the non-cloud obstruction bit would be set. The tri-spectral technique may also be used to flag a region as potentially contaminated with volcanic aerosol. In addition, this bit may be used to pass information on to the aerosol retrieval algorithm.

3.5.5 Thin Cirrus Test (Bits 12 & 16)

VIIRS band M9 (1.38 μm) will use reflectance thresholds on a per pixel basis to detect the presence of thin cirrus cloud in the upper troposphere under daytime viewing conditions. The strength of this cloud detection channel lies in the strong water vapor absorption in the 1.38 μm region. With sufficient atmospheric water vapor present (estimated to be about 0.4 cm precipitable water) in the beam path, no upwelling reflected radiance from the Earth's surface reaches the satellite. Since 0.4 cm is a small atmospheric water content, most of the earth's surface will indeed be obscured in this channel. With relatively little of the atmosphere's moisture located high in the troposphere, high clouds appear bright; reflectance from low and mid level clouds is partially attenuated by water vapor absorption.

Simple low and high reflectance (normalized by incoming solar at the top of the atmosphere) thresholds will be used to separate thin cirrus from clear and thick (near infrared cloud optical depth > ~ 0.2) cloud scenes. These thresholds will be set initially using a multiple-scattering model with the assumption of no surface reflectance contribution to the satellite observed radiance, i.e., a dark background. Ben-Dor (1994) analyzed a scene from the AVIRIS to demonstrate that thin cirrus detection using 1.38 μm observations may be more difficult for elevated surfaces, dry atmospheric conditions, and high albedo surfaces. New injections of volcanic aerosols into the stratosphere may also impact this test.

The MAS 1.88 μm channel is being used as a surrogate to VIIRS channel M9 to gain experience with defining the thin cirrus bit. If the reflectance lies above the clear-sky threshold and less than a thick cloud, then the thin cirrus bit will be set to zero (thin cirrus detected). We subjectively define thin cirrus as a cloud that has a small impact on the visible reflectance, enabling atmospheric correction to be applied to retrieve land surface properties (i.e., NDVI). Figure 1 demonstrates the potential utility of the 1.38 μm channel. The three panels are observations from the MAS during the SUCCESS field campaign. The MAS has a 1.88 μm channel, which like the 1.38 μm channel, is near a strong water vapor absorption band. The panel to the left is a visible image that has been histogram normalized. The right panel is an 11 μm image where dark regions represent cold scenes. The center scene is the 1.88 μm image which clearly shows the presence of contrails that are difficult to see in the 11 μm image and indiscernible in the 0.66 μm image. Given the sensitivity to thin high clouds, the VIIRS 1.38 μm

channel may detect a much larger cloud coverage than previous satellite algorithms have indicated.

3.5.6 Cloud Shadow Test (Bit 11)

The cloud masking algorithm checks for shadows whenever a high confident clear scene is identified. Shadow detection is based on reflectance at 0.87 and 0.66 μm. A shadow is determined present if $R_{0.87}/R_{0.66} > 0.9$.

An example of the results of the shadow algorithm is shown in Figure 8. The left hand panel is a 0.66 μm image, and the right hand panel represents the masking shadow algorithm. Dark regions are shadowed regions; gray, non-shadowed; and white, cloudy scenes.

The issue of shadows caused by mountainous terrain has also been raised. These shadows would be directly calculable from digital elevation maps, solar geometry considerations, and the cloud mask. The first two considerations would indicate the FOVs where terrain shadow could occur; the last would determine whether sunlight is available to cause the shadow. The cloud mask will not separate shadows caused by terrain from those caused by clouds.

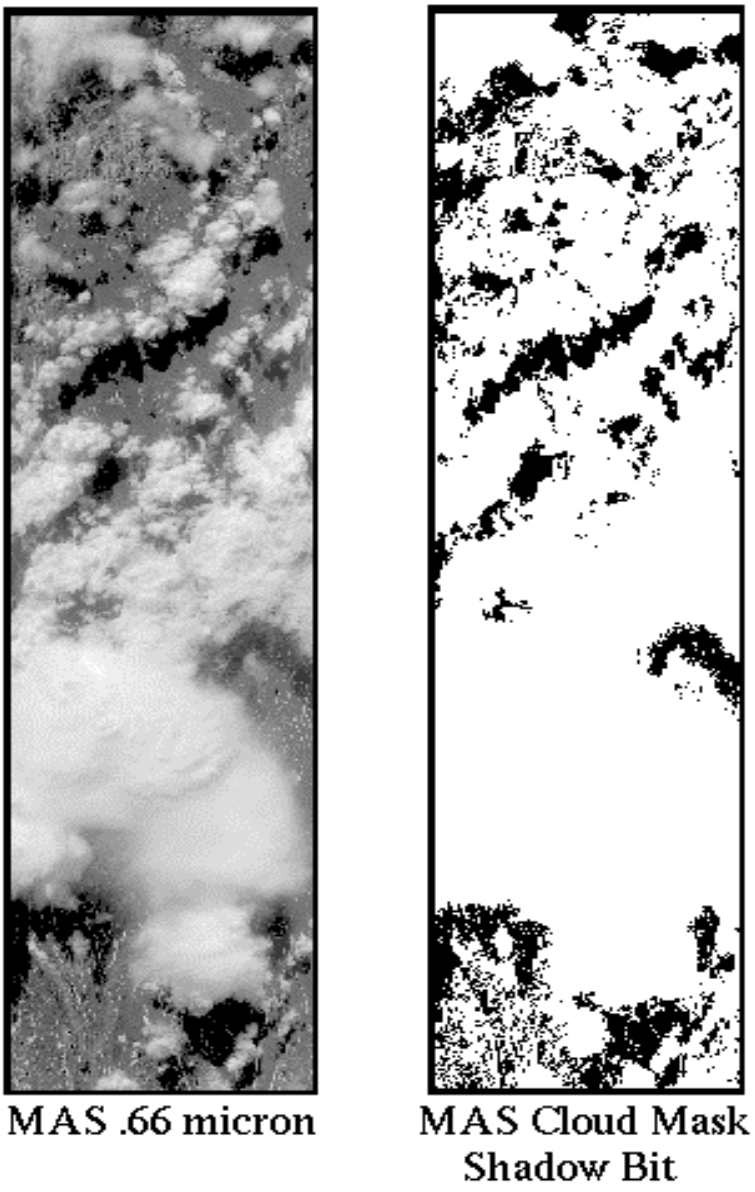

Figure 8 An example of the shadow testing using MAS data over the north slope of Alaska (13 June 1995) The panel to the right demonstrates the results from shadow testing, black regions are shadowed, white areas are cloudy or non-shadowed.

3.5.7 Fire Detection Test (Bit 14)

The fire detection test will follow the MODIS methodology which uses the $BT_{4.05}$ and BT_{11}. For absolute fire detection, the algorithm requires that at least $BT_{4.05} > 360$ K (330 K at night) or $BT_{4.05} > 330$ K (315 K at night) and $BT_{4.05} - BT_{11} > 25$ K (10 K at night) be satisfied. If either of these absolute criteria is not met, the algorithm allows a relative fire detection in which the fire is distinguished from the background by 4 standard deviations in $BT_{4.05}$ and $BT_{4.05}$ - BT_{11}. For daytime observations, a fire pixel is rejected if the VIIRS detects sun glint.

3.5.8 Visible Reflectance Test (Bit 20)

The visible reflectance test is a single channel test whose strength is discriminating bright clouds over dark surfaces (e.g., stratus over ocean) and weakness is clouds over bright surfaces (e.g., snow). Two different channels are used in this test dependent on the ecosystem. The 0.66 μm (band M5) is used over oceans, land and snow/ice regions. The 0.87 μm (band M7) reflectance test is also applied over snow/ice and desert scenes. The nominal thresholds are given below. These thresholds are being set based on observations from AVHRR and MAS.

Table 5 Thresholds used for $R_{0.66}$ - $R_{0.87}$ test for the VCM algorithm

Scene Type	Threshold	High Confidence Clear	Low Confidence Clear
		$R_{0.66}$	
Day Ocean	0.07	0.065	0.08
Day Land	0.16	0.14	0.18
Day Polar	0.20	0.22	0.18
		$R_{0.87}$	
Day Polar	0.10	0.12	0.08
Desert	0.30	0.26	0.34

Figure 9 is an example of MAS observations taken over the tropical ocean.

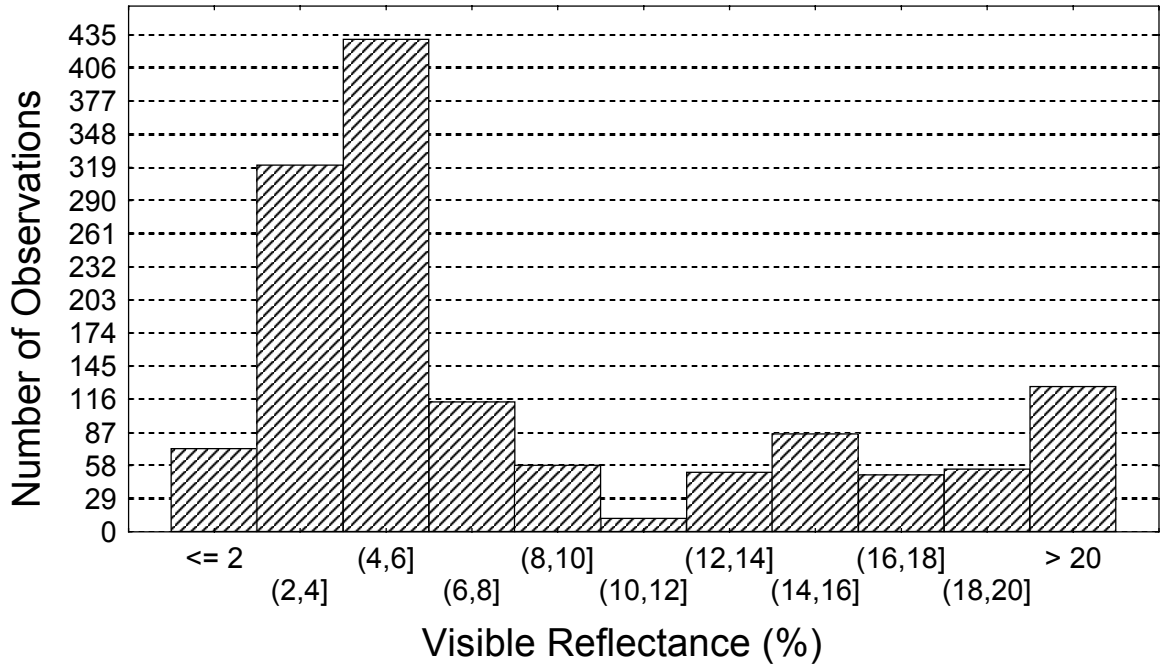

Figure 9 Histogram of the frequency of occurrence of MAS visible reflectance $R_{0.66}$ during part of the TOGA COARE experiment

The reflectance test is view-angle dependent and is also applied in sun glint regions as identified by the sun glint test. Figure 10 demonstrates the angular dependence of the 0.66 μm reflectance test. A histogram analysis of the reflectances from AVHRR data was performed for 1° increments of reflected sun angle, θ_r. The histogram peak, the histogram mean, and the mean value plus 3 standard deviations about the mean reflectance were determined as a function of θ_r. The reflectance thresholds over water are therefore a function of θ_r.

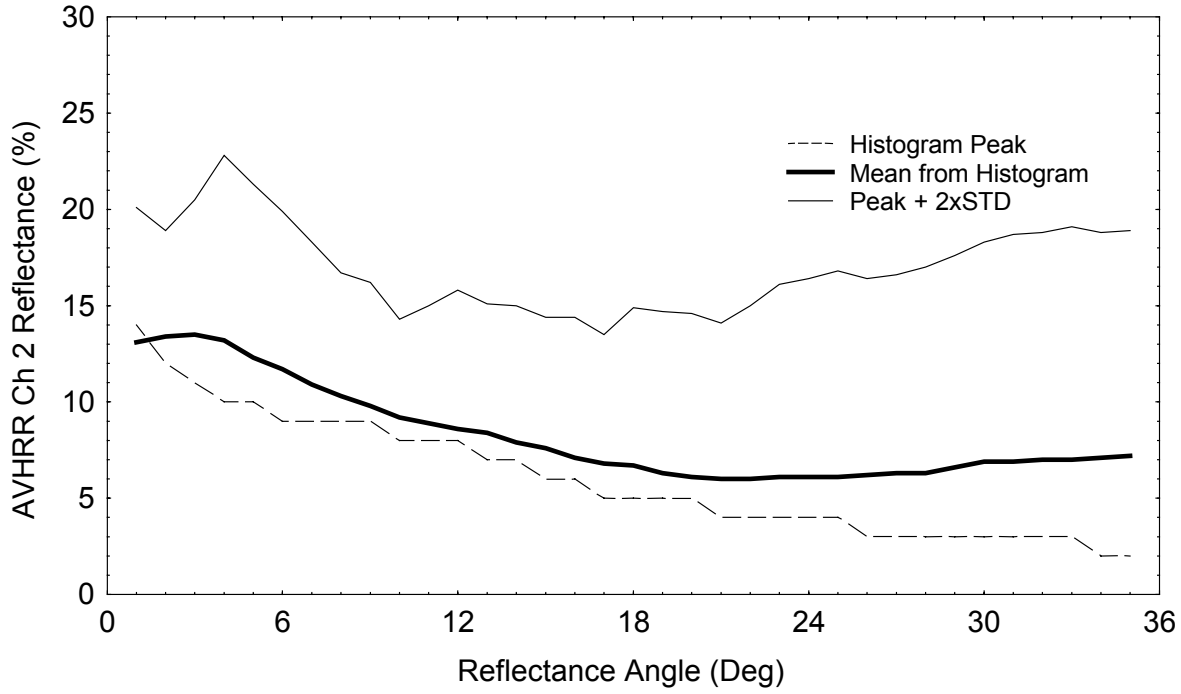

Figure 10 AVHRR channel 2 reflectance as a function of reflectance angle derived from NOAA-14 CHAPS data

3.5.9 Visible Reflectance Ratio Test (Bit 21)

The reflectance ratio test uses channel M7 divided by channel M5 ($R_{0.87}/R_{0.66}$). This test makes use of the fact that the spectral reflectance at these two wavelengths is similar over clouds (ratio is near 1) and different over water and vegetation. Using AVHRR data this ratio has been found to be between 0.9 and 1.1 in cloudy regions. If the ratio falls within this range, a cloud is indicated. New analyses (McClain 1993) suggest that the minimum value may need to be lowered to about 0.8, at least for some cases. For cloud-free ocean the ratio is expected to be less than 0.75 (Saunders and Kriebel 1988). This ratio is generally observed to be greater than 1 over vegetation. Adjustments to the ratio thresholds will be made as necessary for VIIRS data and must be a function of the ecosystem as noted below.

Figure 11 illustrates some of the complexities of desert ecosystems as demonstrated by the visible reflectance ratio. The observations are from the AVHRR on the NOAA-9 and are over the Arabian Sea, the Arabian Peninsula, and surrounding regions. The figure shows histograms of reflectance ratio values for coastal/water scenes, as well as desert and more densely vegetated areas in the Persian Gulf region from approximately 15-25° N latitude and 50-70° E longitude. Almost all of the observations recorded in the histograms were from clear-sky conditions, as determined by inspection of visible and IR imagery. As suggested by the histograms of $R_{0.87}/R_{0.66}$, clear-sky ocean scenes have a ratio of less than 0.75. The surface type classifications are from the Olson World Ecosystems data set. One can immediately see that clear-sky desert

values of the visible reflectance ratio cover a large range of values, including values one might normally associate with cloudy skies over vegetated surfaces. Also note the large amount of overlap between the desert and shrub/grassland categories. This figure shows that clear-sky spectral threshold tests need to be applied very carefully in arid regions and also points out the need for high-resolution ecosystem maps. This test will not be performed over desert, semi-desert, snow/ice, or some agricultural ecosystems.

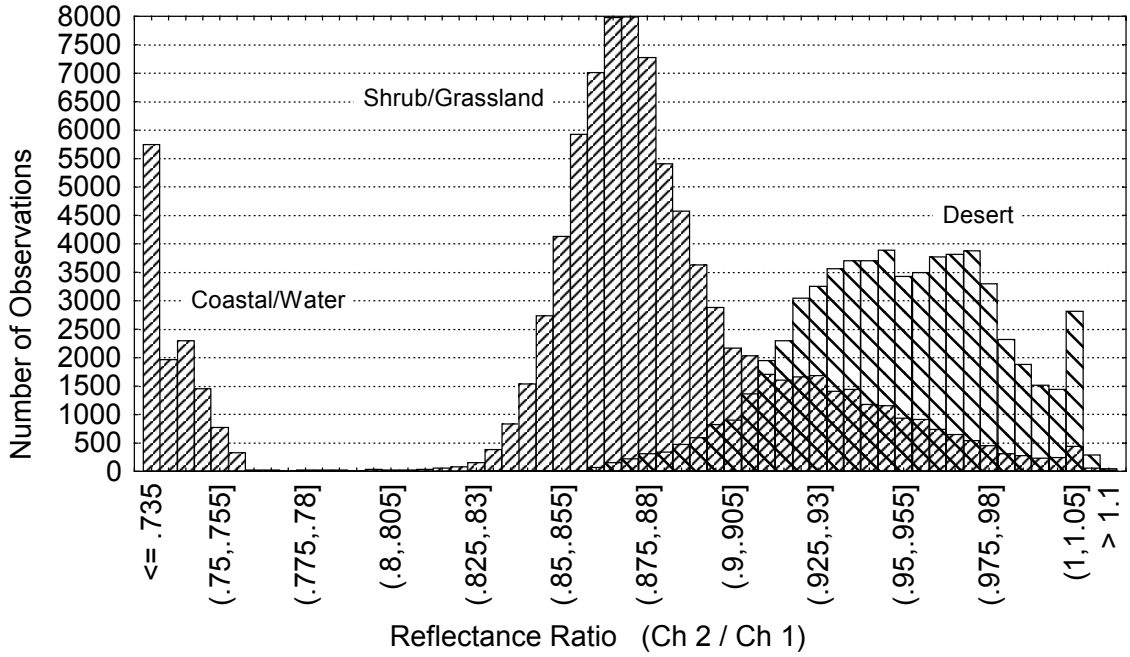

Figure 11 Histogram of the frequency of occurrence of the AVHRR reflectance ratio R0.86/R0.63 for a scene over the Arabian peninsula and Arabian Sea

This reflectance ratio test may also be performed over water during the daytime. When applied in regions of possible sun glint, an angular dependence is included in the thresholds. These thresholds are based on analysis of AVHRR LAC and GAC data and the APOLLO algorithm.

3.5.10 Imagery Band Tests (Bits 23-38)

The imagery bands on the VIIRS sensor are at a finer resolution than the other VIIRS radiometric bands, which they nest within. Presently they are assumed to be bands centered at 0.645, 0.865, 1.61, 3.74, and 11.45 microns, and to have a HSR of approximately 375 meters. Cloud tests performed with these bands will be reported at the imagery resolution, and have spectral contrast tests performed upon them, along with tests being performed at the finest resolution they offer. Imagery band tests will be included in the cloud mask, however; they are not developed at this time.

3.5.11 Confidence Flags

Each of the tests above returns a confidence level ranging from 1 (high confidence that the pixel is clear) to 0 (high confidence that the pixel is cloudy). The individual confidence levels must be combined to determine a final decision on clear or cloudy. We shall denote the confidence level of an individual test as F_i and the final quality flag as Q. There are different methods of combining these individual tests to yield the final quality flag (bits 1 and 2).

The VIIRS Cloud Mask is a clear-sky conservative case. A test with a high confident clear result sets the bit to clear

$$Q = 1 - \prod_{i=1}^{N} [1 - F_i],$$

Several tests are not independent of one another. For example, consider daytime over oceans in regions without sun glint. If stratocumulus clouds are present, they will likely be detected by the visible reflectance test, the reflectance ratio test, and the $BT_{11} - BT_{3.7}$. These same tests will likely miss the presence of thin uniform cirrus clouds, which would probably be detected by the tri-spectral tests (combinations of $BT_{8.7}$, BT_{11}, and BT_{12}). Very thin cirrus clouds would best be detected by the 1.378 test which has difficulty detecting low level clouds. Because of this overlap in the type of clouds different tests detect, each test is considered in one of five groups. The five groups are:

Group I (Simple IR threshold test)

Group II (Brightness temperature difference)

Group III (Solar reflectance tests)

Group IV (NIR thin cirrus)

Group V (IR thin cirrus)

A minimum confidence is determined for each group,

$$G_{i=1,5} = \min[F_i].$$

The final cloud mask is then determined from the product of the results from each group;

$$Q = \sqrt[N]{\prod_{i=1}^{N} G_i}\ .$$

This approach is considered clear-sky conservative. If any test is highly confident that the scene is cloudy ($F_i = 0$), the final cloud mask is $Q = 00$.

The algorithm is divided into eight conceptual domains according to surface type and solar illumination:

1. Daytime land,
2. Daytime water,
3. Nighttime land,
4. Nighttime water,
5. Daytime desert,
6. Nighttime desert,
7. Daytime snow/ice covered regions, and
8. Nighttime snow/ice covered regions.

"Daytime" is defined as a solar zenith angle $\theta_0 < 85°$ (and the instrument is in daytime mode). The "desert" classification is based on the 10-minute Olson World Ecosystems data set. A USGS 1 km land/sea tag file is used for land/water discrimination. For all observations within a given domain, it is generally expected that: (i) the same tests may be performed, and (ii) threshold values for each of these tests will not change. It is expected that more domains may be established in the future.

3.6 PRACTICAL CONSIDERATIONS

3.6.1 Numerical Computation Considerations

Bispectral cloud detection tests are computationally inexpensive. However, it is important that pixels are only detected as cloud a single time; therefore, the most efficient cloud detection test is applied first to all pixels. Those pixels classified as cloud-contaminated are removed, flagged, and the second cloud test is applied only to those remaining cloud-free, and so forth. Adjustments for special effects, e.g., partially cloudy pixels and shadows, are made only after all cloud tests have been applied and pixels identified as cloud-contaminated have been flagged.

3.6.2 Programming and Procedural Considerations

The procedural outline has been described in Section 3.1.

3.6.3 Configuration of Retrievals

To avoid "hard-wiring" specific values into the operational software, a retrieval configuration file can be adopted. The file would store numerical values of adjustable parameters used within the retrievals, such as the thresholds establishing whether a successful retrieval occurs.

3.6.4 Quality Assessment and Diagnostics

Bit 0 of the VIIRS Cloud Mask output is a quality flag indicating whether the cloud mask result is questionable (0) or okay (1). Additional information regarding the VIIRS Cloud Mask quality can be found in Section 3.3.1.

3.6.5 Exception Handling

VIIRS will produce a cloud mask under all circumstances. Processing performed on questionable input data will be highlighted with the quality flag indicator in the final output.

3.7 ALGORITHM VALIDATION

The VIIRS cloud mask algorithm will be verified pre-launch using data from existing satellite systems, such as Advanced Very High Resolution Radiometer (AVHRR) and MODIS. More pre-launch validation will be performed along with the update of detection modules. Post-launch verification will involve intercomparisons between VIIRS observations, ground-based measurements, and special airborne campaigns.

3.8 ALGORITHM DEVELOPMENT SCHEDULE

The algorithm for the VIIRS cloud mask is of MODIS heritage, with the exception of tests performed using bands not common to MODIS. Development of this algorithm is under way. The methods will be verified using MODIS global data as it becomes available. The similarity of the proposed VIIRS bands to the MODIS bands make MODIS data a reliable verification source.

4 ASSUMPTIONS AND LIMITATIONS

4.1 ASSUMPTIONS

(1) Cloud Mask receives an image of VIIRS calibrated and geolocated TOA reflectances and TOA BT's in the bands used by the Cloud Mask, including any Imagery bands used.

(2) Cloud Mask receives an image of calibrated and geolocated TOA DNB reflectances.

(3) Quality flags accompany all input data into the Cloud Mask Module indicating if the data is good, bad, or questionable.

(4) Cloud Mask receives Geolocated Latitudes and Longitudes of all pixels in the region being masked.

(5) Cloud Mask receives an entire image of the region being masked.

(6) Cloud Mask needs a Land/Water reference database.

(7) Cloud Mask needs an ecosystem reference database.

(8) Cloud Mask receives Sun Sensor geometry.

(9) Cloud Mask receives a database of recent snow/ice knowledge either from CMIS or the previous 12 hour VIIRS Snow/Ice Cover EDR.

(10) Output mask results will have 4 levels of confidence. Confident Cloudy, Probably Cloudy, Probably Clear, and Confident Clear.

(11) Cloud Mask receives Sea surface wind data in region being masked for determination of Sun Glint Flag.

(12) Ecosystem database received by cloud mask contains forest surface type.

(13) Band Nesting is assumed.

4.2 LIMITATIONS

(1) Can only produce Cloud Mask if BT and Reflectance data are available.

(2) Can only produce Cloud Mask if underlying surface type is known.

(3) Cloud and Snow/Ice Mask will be produced at the spatial resolution of all bands employed.

5 REFERENCES

Ackerman, S. A., W. L. Smith and H. E. Revercomb (1990). The 27-28 October 1986 FIRE IFO Cirrus Case Study: Spectral Properties of Cirrus Clouds in the 8-12 Micron Window. *Mon. Wea. Rev*., 118, 2377-2388.

Ackerman, S. A., (1996). Global satellite observations of negative brightness temperature difference between 11 and 6.7 μm. *J. Atmos. Sci.*, 53, 2803-2812.

Ackerman, S. A., K. Strabala, P. Menzel, R. Frey, C. Moeller, L. Gumley, B. Baum, C. Schaaf, and G. Riggs (1997). Discriminating Clear-Sky From Cloud With MODIS Algorithm Theoretical Basis Document (MOD35). Version 3.2

Ben-Dor, E., (1994). A precaution regarding cirrus cloud detection from airborne imaging spectrometer data using the 1.38 μm water vapor band. *Remote Sens. Environ.*, 50, 346-350.

Berk, A., L. S. Bernstein, and D. C. Roberson (1989). MODTRAN: A Moderate Resolution Model for LOWTRAN7, Report AFGL-TR-89-0122 (Air Force Geophysics Laboratory), Hanscom, AFB, MA 01731.

Gao, B. C., A. F. H. Goetz, and W. J. Wiscombe (1993). Cirrus Cloud Detection From Airborne Spectrometer Data Using the 1.38 Micron Water Vapor Band, *Geophys. Res. Lett*., 20, 301-304.

Goodman, A. H., and A. Henderson-Sellers (1988). Cloud Detection Analysis: A Review of Recent Progress. *Atm. Res*., 21, 203.

Gustafson, G. B., R. G. Isaacs, R. P. d'Entremont, J. M. Sparrow, T. M. Hamill, C. Grasotti, D. W. Johnson, C. P. Sarkisian, D. C. Peduzzi, B. T. Pearson, V. D. Jakabhazy, J. S. Belfiore, and A. S. Lisa (1994). Support of Environmental Requirements for Cloud Analysis and Archive (SERCAA): algorithm descriptions, PL-TR-94-2114, Phillips Laboratory, AFMC, Hanscom AFB, MA.

Hall, D. K., G. A. Riggs, and V. V. Solomonson (1995). Development of Methods for Mapping Global Snow Cover Using Moderate Resolution Imaging Spectroradiometer Data. *Remote Sens. Env*., 54, 127-140.

Hall, D. K., G. A. Riggs, and V. V. Solomonson (1996). Algorithm Theoretical Basis Document (ATBD) for the MODIS Snow-, Lake Ice-, and Sea Ice-Mapping Algorithms. Version 3.0.

Hutchison, K. D., and K. Hardy (1995). Threshold functions for automated cloud analyses of global meteorological satellite imagery. *International Journal of Remote Sensing,* 16, 3665-3680.

Hutchison, K. D., and N. Choe (1996). Application of 1.38 μm imagery for thin cirrus detection in daytime imagery collected over land surfaces. *International Journal of Remote Sensing,* 17, 3325-3342.

Hutchison, K. D., and J. K. Locke (1997). Snow Identification through Cirrus Cloudy Atmospheres using AVHRR Daytime Imagery. *Geophysical Research Letters*, 24, 1791-1794.

Hutchison, K. D., B. J. Etherton, and P. C. Topping (1997). Validation of automated cloud top phase algorithms: distinguishing between cirrus clouds and snow in a-priori analyses of AVHRR imagery. *Optical Engineering*., 36, 1727-1737.

Hutchison, K. D., B. J. Etherton, P. C. Topping, and A. H. L. Huang (1997). Cloud Top Phase Determination from the Fusion of Signatures in Daytime AVHRR Imagery and HIRS Data. *International Journal of Remote Sensing*, 18, 3245-3262.

Hutchison, K. D., K. Hardy, and B. C. Gao (1995). Improved detection of optically-thin cirrus clouds in nighttime multispectral meteorological satellite imagery using total integrated water vapor information. *Journal of Applied Meteorology,* 34, 1161-1168.

Inoue, T., (1987). A cloud type classification with NOAA 7 split window measurements. *J. Geophys. Res*., 92, 3991-4000.

King, M. D., W. P. Menzel, P. S. Grant, J. S. Myers, G. T. Arnold, S. E. Platnick, L. E. Gumley, S. C. Tsay, C. C. Moeller, M. Fitzgerald, K. S. Brown, and F. G. Osterwisch (1996). Airborne Scanning Spectrometer for Remote Sensing of Cloud, Aerosol, Water Vapor, and Surface Properties. *J. Atmos. Oceanic Technol*., 13, 777-794.

Kriebel, K. T., and R. W. Saunders (1988). An Improved Method for Detecting Clear Sky and Cloudy Radiances from AVHRR Data. *Int. J. Remote Sens*., 9, 123-150.

Lou, G., P. A. Davis, L. L. Stowe, and E. P. Mcclain (1995). A pixel-scale algorithm of cloud type, layer, and amount for AVHRR data. Part I: Nighttime, *Journal of Atmospheric and Oceanic Technology*, 12, 1014-1036.

McClain, E. P. (1993). Evaluation of CLAVR Phase-I Algorithm Performance: Final Report, U.S. Department of Commerce/NOAA/NESDIS. Report 40-AANE-201-424.

Rossow, W. B. (1989). Measuring Cloud Properties from Space: A Review. *J. Clim*., 2, 201.

Saunders, R. W. and K. T. Kriebel, (1988). An improved method for detecting clear sky and cloudy radiances from AVHRR data, *International Journal of Remote Sensing,* 9, 123-150.

Stamnes, K., W. Li, X. Xiong, and B. Chen (1998). Remote Sensing of Cloud and Surface Properties in Polar Regions from GLI Measurements on Board ADEOS-II. The 3rd GLI Workshop, Tokyo.

Stowe, L. L., P. Davis, and E. P. McClain (1995). Evaluating CLAVR (Clouds from AVHRR) Phase I Cloud Cover Experimental Product. *Adv. in Space Res*., 16, 21-24.

Stowe, L. L., P. Davis, and E. P. McClain (1998). Scientific Basis and Initial Evaluation of the CLAVR-I Global Clear/Cloud Classification Algorithm for the Advanced Very High Resolution Radiometer, *J. Atmos. and Oceanic Technology*, submitted May 1st.

Strabala, K. I., S. A. Ackerman, and W. P. Menzel (1994). Cloud Properties Inferred from 12 micron Data, *J. Appl. Meteor*., 33, 212-229.

Valvocin, F. R. (1978). Spectral radiance of snow and clouds in the near infrared spectral region. *Tech Report No. 78-0289*, Air Force Geophysics Laboratory, Hanscom Air Force Base, MA.

Yamanouchi, T., K. Suzuki, and S. Kawaguci, (1987). Detection of clouds in Antarctica from infrared multispectral data of AVHRR. *J. Meteor. Soc. Japan*, 65, 949-962.